

Journal of Materials Chemistry A

Accepted Manuscript



This is an *Accepted Manuscript*, which has been through the Royal Society of Chemistry peer review process and has been accepted for publication.

Accepted Manuscripts are published online shortly after acceptance, before technical editing, formatting and proof reading. Using this free service, authors can make their results available to the community, in citable form, before we publish the edited article. We will replace this *Accepted Manuscript* with the edited and formatted *Advance Article* as soon as it is available.

You can find more information about *Accepted Manuscripts* in the [Information for Authors](#).

Please note that technical editing may introduce minor changes to the text and/or graphics, which may alter content. The journal's standard [Terms & Conditions](#) and the [Ethical guidelines](#) still apply. In no event shall the Royal Society of Chemistry be held responsible for any errors or omissions in this *Accepted Manuscript* or any consequences arising from the use of any information it contains.

Synthesis of Hierarchically Nanostructured TiO₂ Spheres with Tunable Morphologies Based on a Novel Amphiphilic Polymer Precursor and Their Use for Heavy Metal Ion Sequestration

Wei Sun, Min Chen, Shuxue Zhou and Limin Wu*

Received (in XXX, XXX) Xth XXXXXXXXXX 20XX, Accepted Xth XXXXXXXXXX 20XX

DOI:

ABSTRACT: TiO₂ has many important applications, but its structures and morphologies are usually difficult to turn due to the uncontrollable and fast sol-gel reactions of current TiO₂ precursors. This paper presents a facile and general method for fabrication of hierarchically nanostructured TiO₂ spheres with controllable morphologies based on a novel amphiphilic polymeric TiO₂ precursor. By adjusting the conditions of hydrolysis and condensation reactions of this precursor, TiO₂ spheres with various morphologies, including hierarchical porous, hollow, and raspberry-like structures, can be produced easily. The as-obtained spheres have hierarchical structures with specific surface areas larger than 200 m² g⁻¹ and mean pore sizes of several nanometers. Mechanism study indicates that the amphiphilic polymer assistant aggregation, abrupt, migration, and crystallization of certain TiO₂ units during hydrolysis and condensation process contribute to the formation of TiO₂ spheres with various morphologies. The as-obtained specific hierarchically nanostructured TiO₂ spheres exhibit considerably higher adsorption capability for Cr (VI) anions in aqueous solution compared with the previously reported TiO₂ nanomaterials, showing a high potential for heavy metal ion sequestration applications.

Introduction

TiO₂ nanoparticles, which are often treated as representative nanomaterials, have been extensively investigated over the past few decades because of their excellent physicochemical properties. They have important applications in many fields, such as dye-sensitized solar cells,¹ photocatalyses,² self-cleaning and wettability-tunable coatings,³ phosphorylated protein enrichment,⁴ and gas sensors.⁵

There are generally two kinds of strategies for the fabrication of TiO₂ nanomaterials: one is based on physical methods, another on chemical processes. The latter has been widely used in the fabrication of TiO₂-based materials due to its low cost and ease of operation.⁶⁻¹² Many chemical strategies, such as sol-gel, templating synthesis, thermolysis, solvothermal and self-assembly have been developed for the fabrication of TiO₂ nanoparticles.^{12,13} Among these reported chemical methods, the sol-gel technology is particularly interesting and the most effectively used.¹⁴ Nevertheless, the current sol-gel methods of all the TiO₂ precursors reported cannot be used for preparation of TiO₂ spheres with tunable structures or morphologies because all these precursors are monomeric and have too fast hydrolysis and condensation reactions which are hardly controlled.^{8,15} This greatly restricts the applications of both the sol-gel method and TiO₂ nanoparticles. Therefore, it is highly desirable to explore low-cost facile methods to prepare TiO₂ nanoparticles with tunable structures and morphology theoretically and technologically.

As is well established, amphiphilic block copolymers can self-assemble into many micro phase-separated micelles in different

structures on the scale of dozens of nanometers up to several microns in selective solvents.¹⁶ The capacity to self-assemble can greatly facilitate the integration of nanotechnology with other technologies and, in particular, with microscale fabrication. The aggregations of various morphologies not only decrease the free energy of system, but provide excellent templates for the organization of the nanoparticles with different superstructures.¹⁷ Eiden-Assmann *et al.* and Zhao *et al.* ever successfully fabricated monodisperse colloidal TiO₂ spheres and mesoporous structured TiO₂ by adding appropriate amphiphilic copolymers during the sol-gel process of monomeric TiO₂ precursors using physical mixing method.¹⁸⁻¹⁹ The as-formed micelles which consist of a lyophobic core formed from the insoluble blocks and a lyophilic corona formed from the soluble blocks help to guide the final structures of TiO₂ materials. However, because the precursors and copolymers were only connected by non-covalent bonds, such as hydrogen bond and hydrophobic interactions, the assembly behaviors of amphiphilic copolymers had a limited effect on the sol-gel process of these monomeric precursors. As a result, only single morphology had been obtained. Recently, Wang *et al.* fabricated mesostructured silica spheres by hydrolysis of a polymeric silica precursor, which was synthesized from modification of hyperbranched polyethoxysiloxane (PEOS) with poly(ethylene glycol) (PEG). The morphologies of the as-formed silica spheres could be turned from mesoporous particles, hollow spheres to ultrasmall solid particles by adjusting the amount of PEG used.²⁰ However, due to the relatively mild sol-gel reaction of silica precursors, it still remains a big challenge to extend this method to fabrication of TiO₂ and other inorganic oxides.

Heavy metal ions in water bring many detrimental effects on environment and human health. Recently the exploitation of metal oxides for heavy metal ion and radwaste sequestration has attracted much attention because of their superior thermal, chemical, hydrolytic and radiolytic stabilities and outstanding durability.²¹ Many metal oxides, such as zirconium titanium oxide,^{22,23} TiO₂,^{24,25} ceria (CeO₂),²⁶ iron oxide^{27,28} *etc.*, with

Department of Material Science and State Key Laboratory of Molecular Engineering of Polymers, Fudan University, Shanghai 200433, China
*Email: lmw@fudan.edu.cn

various morphologies have been fabricated and taken for heavy metal ion sequestration applications. For example, Wan *et al.* prepared 3D flowerlike nanostructures of iron oxide using an ethylene-glycol-mediated self-assembly process and the as-obtained materials showed very good ability to remove various heavy metal ions from water.²⁸ Caruso *et al.* prepared monodisperse mesoporous zirconium titanium oxide microspheres with varying compositions, and the resultant microspheres showed very high adsorption capacities for Cr (VI) anions from solution.²² As is well known, TiO₂ materials are typical materials for photocatalytic degradation of pollutants due to their excellent photoelectric properties. As a result, if could be endowed with better heavy metal ion sequestration capability, accordingly, the application fields and performances of TiO₂ materials for water treatment and other environmental protection will be absolutely promoted. On the other hand, the adsorption capacity of adsorbents is strongly affected by their specific surface areas and the morphologies. Among various reported morphologies, the hierarchically nanostructured spherical metal oxides with high surface to bulk ratio, high pore volumes, large surface area, facile mass transportation ability and unique packing ability are recognized the most promising performances for the removal of heavy metals from aqueous solutions.^{21,22} Recently, Moon *et al.* synthesized hierarchically nanoporous magnesia (MgO) and ceria CeO₂ based on a metal-organic framework (MOF)-driven, self-templated route.²⁹ The as-obtained materials were in bulk rather than spherical structures. Besides, it is still very difficult to extend this method for the synthesis of hierarchically nanostructured TiO₂ materials due to the furious and uncontrollable hydrolysis and condensation reactions of traditional TiO₂ precursors.

In this study, we present a facile strategy for the fabrication of hierarchically nanostructured TiO₂ spheres with tunable morphologies based on the sol-gel reaction of a novel designed amphiphilic polymeric TiO₂ precursor. This precursor was synthesized through an amphiphilic block polymer, polyethylene glycol hexadecyl ether (PEGHE) chemically grafting onto a typical monomeric TiO₂ precursor—titanium tetraisopropoxide (Ti(OⁱPr)₄). Compared with the previously monomeric TiO₂ precursors and their sol-gel reaction for TiO₂ spheres,^{30,31} the present approach has following merits: i) The hydrolysis and condensation reactions of this new hybrid precursor are controllable and mild, which are impossible achievable for monomeric TiO₂ precursors; ii) This hybrid precursor and its sol-gel reaction can be easily used for synthesis of hierarchically nanostructured TiO₂ spheres with tunable morphologies, which have been little obtained through current strategies; iii) Owing to their high specific surface areas, narrow pore size distributions and specific surface properties, the as-prepared hierarchically nanostructured TiO₂ spheres have very high adsorption capability for Cr (VI) anions in aqueous solution.

Experimental procedure

Materials

Amphiphilic block copolymer (PEGHE, C₁₆H₃₃(OCH₂)₁₀OH) was purchased from Aldrich. Titanium tetraisopropoxide (Ti(OⁱPr)₄), 1-(2-pyridinylazo)-2-naohtalenol, cadmium nitrate (Cd(NO₃)₂) and potassium dichromate (K₂Cr₂O₇) were purchased from

Aladdin Chemical Reagent Corp. Ethanol and 1,5-diphenylcarbazine were purchased from Sinopharm Chemical Reagent Corp. A typical commercially available nano-TiO₂ powder (Degussa P-25) was from Degussa Corp (Germany). Millipore water was used for solution preparation and synthesis in all experiments.

65 Synthesis of amphiphilic polymer/inorganic hybrid TiO₂ precursor

PEGHE (6.83 g, 10 mmol) was charged a flask and heated to 40 °C to melt it. Then Ti(OⁱPr)₄ (2.84 g, 10 mmol) was quickly added to the flask with vigorous stirring. This mixture was held at 40 °C under intensive stirring and the resultant isopropyl alcohol was fractionated off continuously in vacuum. The heat supply was continued until the distillation of isopropyl alcohol stopped. The product was finally cooled down and kept in a refrigerator.

75 Synthesis of TiO₂ spheres with tunable morphologies

Typically, the hybrid precursors (0.1 g) were added to 5 mL of mixture solvent of ethanol and water (volume ratio: 4:1) at room temperature under vigorous stirring. After being stirred for another 30 min, the resultant colloidal suspension of TiO₂ was centrifuged and washed with the same type of solvent for 3 cycles. Then the TiO₂ was re-dispersed into this mixture solvent (40 mL) and further aged at 160 °C for 15 h. After that, this mixture was cooled down and the precipitates were collected and washed 3 times with the same type of solvent and dried at 30 °C in a vacuum. After calcination at 400 °C in air for 2 h, hierarchical porous TiO₂ spheres were obtained.

When the aging temperature was fixed 75 °C but other parameters remained equal, hollow TiO₂ spheres formed.

When the amphiphilic polymer-modified TiO₂ hybrid precursors and mixture solvent were mixed and stirred at 75 °C for 10 min and then aged at 75 °C for 15 h, raspberry-like TiO₂ spheres were synthesized.

Heavy metal ion adsorption experiments

Cr (VI) adsorption experiments were performed using batch contact methodology with K₂Cr₂O₇ as the sources of Cr (VI). The pH value of the K₂Cr₂O₇ solution was adjusted to 3 with 0.1 M HNO₃ prior to the adsorption experiments. 20 mg of samples were suspended in 10 mL K₂Cr₂O₇ solution with different initial Cr (VI) concentrations (5, 10, 20, 50, 100 and 200 mg/L) and stirred for 24 h. After the adsorption processes, the solid was removed by centrifugate and the supernatant was immediately analyzed by UV-vis spectrophotometer using 1,5-diphenylcarbazine as the chromogenic reagent at the wavelength of 542 nm. For Cd (II) adsorption, Cd(NO₃)₂ and 1-(2-pyridinylazo)-2-naohtalenol were used as the sources of Cd (II) and the chromogenic reagent, respectively, and were monitored by UV-vis spectrophotometer at the wavelength of 552 nm.³²

For regeneration, K₂Cr₂O₇ solution with initial Cr (VI) concentrations of 10 mg/L was used in all cases. The Cr (VI) adsorbed samples were immersed in 5 mL of NaOH solution (0.1 mol/L) for 5 h and then the solid was washed with DI water for five times to remove adsorbed alkali. The Cr (VI) adsorption test was then repeated on the separated adsorbents by the method described above to test the reusability of the materials.

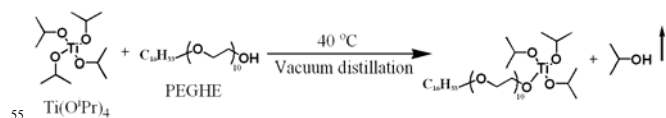
Characterization

Transmission electron microscopy (TEM) images were taken with a Philips CM200FEG field emission microscope. Scanning electron microscopy (SEM) and energy dispersive X-Ray spectroscopy (EDX) were conducted for microanalysis with a Philips XL 30 field emission microscope equipped with a thin window EDX system with energy dispersion spectrometry at an accelerating voltage of 10 kV. Dynamic light scattering (DLS) measurements were carried out on the diluted reaction solutions to produce particles of average diameter and size distribution using a Nano-ZS90 (Malvern). Proton nuclear magnetic resonance (^1H NMR) measurements were carried out on a Bruker (500 MHz) NMR instrument. XRD was conducted in a Rigaku D/max-kA diffractometer with Cu $K\alpha$ radiation. Nitrogen adsorption-desorption isotherms were determined at 77 K using an ASAP 2010 analyzer. Surface area was calculated using the Brunauer-Emmett-Teller (BET) method, and the pore volumes and pore size distributions were obtained using the Barrett-Joyner-Halenda (BJH) model. The UV visible adsorption spectra (UV-vis) were obtained using Hitachi U-4100 spectrophotometry. Thermogravimetry analysis (TGA) was performed using a TGA instrument (Perkin-Elmer TGA-7) from room temperature to 700°C at a rate of 20 °C min^{-1} . The surface composition of film was measured using X-ray photoelectron spectroscopy (XPS, Perkin-Elmer PHI 5000C ECSA) with Al K radiation at a 90° take-off angle. All binding energy values were calibrated using the reference peak of C1S at 284.6 eV.

Results and discussions

Synthesis of amphiphilic polymer/inorganic hybrid TiO_2 precursor

This new hybrid TiO_2 precursor was synthesized through the reaction of equimolar $\text{Ti}(\text{O}^i\text{Pr})_4$ and PEGHE in vacuum at 40 °C, which produced a large number of bubbles to be distilled out due to the formation of isopropanol, as shown in **Scheme 1**. The structure of this novel precursor was characterized by ^1H NMR. As shown in **Fig. 1a**, after the reaction, the peak at 2.14 ppm for the hydroxyl groups of PEGHE disappeared, and the peak of isopropoxide of $\text{Ti}(\text{O}^i\text{Pr})_4$ shifted from 4.49 to 4.02 ppm completely. Because monomeric $\text{Ti}(\text{O}^i\text{Pr})_4$ has four equal functional groups, the degree of functionalization can vary from 0–4 under different conditions, and it can be calculated from the molar ratio of isopropoxide groups (4.02 ppm) of $\text{Ti}(\text{O}^i\text{Pr})_4$ to the methyl groups (0.88 ppm) of PEGHE. Due to the steric effect, the tri- and tetra-adduct can be ignored in this experiment. In this way, the hybrid TiO_2 precursor contains 93% of mono-adduct and only 7% of di-adduct. Besides, as shown in **Fig. S1**, ^1H NMR characterization of $\text{Ti}(\text{O}^i\text{Pr})_4$ reacted with twice and four mole ratio of PEGHE was also conducted, further proving good selectivity of this reaction. The UV-vis spectrum in **Fig. 1b** indicated a considerable blue shift in the wavelength of the absorbance peak, from 265 to 255 nm after the reaction, further confirming the successful grafting of the amphiphilic polymer chains onto $\text{Ti}(\text{O}^i\text{Pr})_4$.



Scheme 1. Chemical modification of titanium tetraisopropoxide ($\text{Ti}(\text{O}^i\text{Pr})_4$) with amphiphilic block copolymer PEGHE ($\text{C}_{16}\text{H}_{33}(\text{OCH}_2)_{10}\text{OH}$).

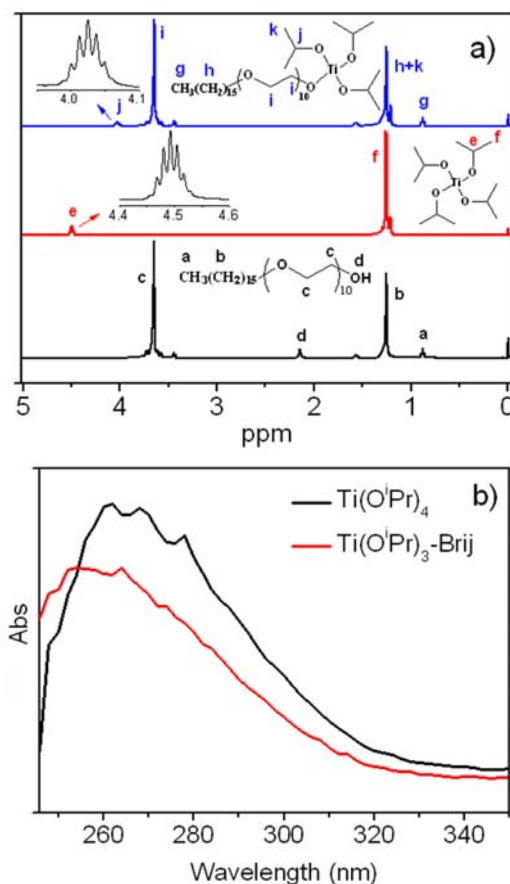


Fig. 1 Characterizations of amphiphilic polymer-modified TiO_2 hybrid precursor. (a) ^1H NMR spectra of PEGHE (black line), titanium tetraisopropoxide ($\text{Ti}(\text{O}^i\text{Pr})_4$) (red line) and the amphiphilic polymer-modified TiO_2 hybrid precursor (blue line) in CDCl_3 . (b) UV-vis spectra of $\text{Ti}(\text{O}^i\text{Pr})_4$ (black) and the amphiphilic polymer-modified TiO_2 hybrid precursor (red) in dichloromethane.

Synthesis of TiO_2 spheres with tunable morphologies

The as-obtained amphiphilic polymer TiO_2 precursors were then hydrolyzed in a mixture solvent of ethanol and water at room temperature. Different hydrolysis and assembly behaviors of the hybrid precursors were observed. These appeared to depend upon the volume ratios of ethanol and water in the solvent. When appropriate volume ratios of ethanol and water, ranging from 9:1 to 4:6, were used, turbid dispersions were observed, as shown in **Fig. 2a**. The corresponding TEM images showed that the as-obtained particles (these particles are called TiO_2 precursor beads in this study) derived from the hydrolysis of hybrid precursors had irregular spherical shapes, and the mean sizes of these beads could be changed from 250 nm to 12 nm by simply changing the ratios of ethanol and water in the mixture solvent (**Fig. 2b–g**). Besides, as shown in **Fig. S2**, the hydrodynamic diameters of the TiO_2 precursor beads were also measured by DLS and similar sizes were obtained compared with those by TEM. The more water the mixture solvent contained, the smaller the TiO_2

precursor beads were. When too much water was used (>60% by volume), however, macroscopic gelation formed (the last three vials in Fig. 2a). This may be due to the excessive speed of hydrolysis of TiO₂ precursor even after having been modified by the amphiphilic polymer. Without water, the amphiphilic-polymer-modified TiO₂ hybrid precursor was soluble in ethanol and formed a transparent solution (the first vial in Fig. 2a), and no particles were observed by TEM.

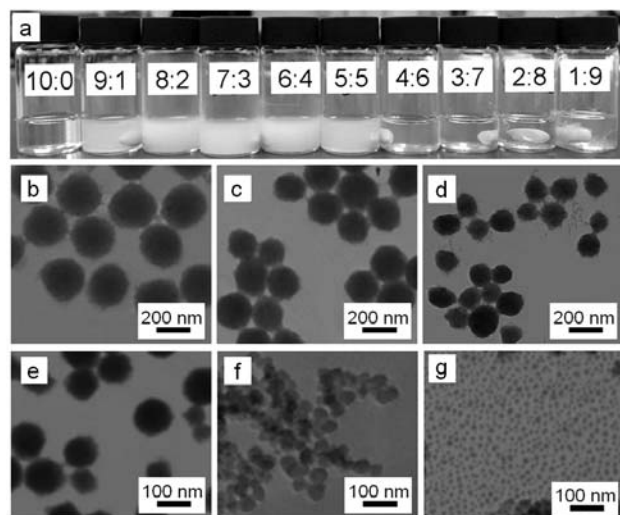


Fig. 2 (a) Digital images of 2 wt% dispersions of amphiphilic polymer-modified TiO₂ precursors hydrolyzed in various volume ratios of ethanol and water (inset numbers: volume ratio of ethanol and water). b–g) TEM images of the TiO₂ precursor beads obtained with varying volume ratios of ethanol and water, corresponding to the samples in the digital images: (b) 9:1; (c) 8:2; (d) 7:3; (e) 6:4; (f) 5:5; (g) 4:6.

When the as-obtained TiO₂ precursor beads were further aged at 160 °C for 15 h, neither TiO₂ spheres similar in size to TiO₂ precursor beads nor spheres similar in size to agglomerates were produced. Instead, much larger spherical TiO₂ particles with peculiar hierarchical porous structures formed. As shown in Fig. 3a–b, the mean diameter of these spheres was $1.7 \pm 0.3 \mu\text{m}$ with the sub-pores of 100–200 nm across each sphere. Careful observation of the magnified image showed that these large TiO₂ spheres were made of small nanoparticles, 12 nm in diameter (here called as TiO₂ primary nanoparticles) (Fig. 3c). Shell thickness was about 80 nm. It was composed of about 6 layers of TiO₂ primary nanoparticles. The sub-pores were connected to each other by around 25 nm thick TiO₂ wall.

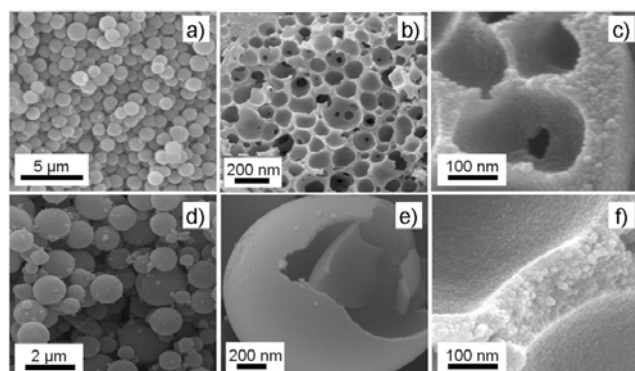


Fig. 3 SEM images of a–c) hierarchical porous TiO₂ spheres, and d–f) hollow

TiO₂ spheres with different magnitudes.

If the as-obtained TiO₂ precursor beads were aged at 75 °C for 15 h, hollow TiO₂ spheres were produced (Fig. 3d–f). Like those of hierarchical porous TiO₂ spheres, the shells of the TiO₂ hollow sphere were also assembled from 12 nm TiO₂ primary nanoparticles, and the mean diameter of these spheres was $2.4 \pm 0.6 \mu\text{m}$ with around 70 nm thick shells, which were composed of about 5 layers of primary nanoparticles. Both the hierarchical porous and the hollow structures were well preserved after calcination. All the TiO₂ precursor beads in Fig. 2b–g produced the similar structure and morphology for final TiO₂ spheres after treatment using the same procedures, suggesting that the size of the TiO₂ precursor beads had little influence on the final morphology and size of TiO₂ spheres.

On the other hand, when the initial sol-gel reaction of the TiO₂ hybrid precursors was conducted at 75 °C in the type of solvent described above, followed by aging at 75 °C for 15 h and calcination at 400 °C, TiO₂ spheres with raspberry-like morphologies were fabricated, as shown in Fig. 4. At a 9:1 ethanol to water ratio, the mean diameter of TiO₂ spheres is 300 nm. By simply changing the volume ratios of ethanol and water in the mixed solvent, raspberry-like TiO₂ spheres of different sizes, from 300 to 15 nm, can be produced easily. These raspberry-like TiO₂ spheres are also composed of primary TiO₂ nanoparticles about 15 nm in diameter.

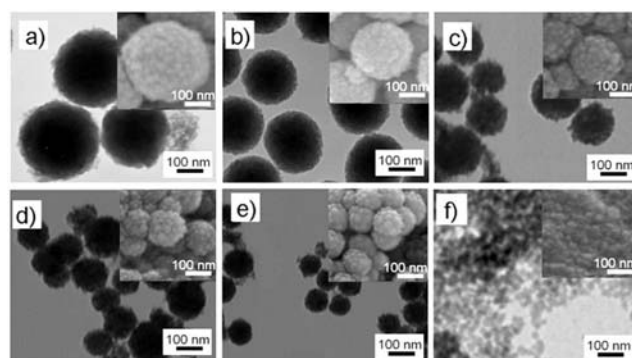


Fig. 4 TEM and the inserted SEM images of raspberry-like TiO₂ spheres synthesized with varying ethanol: H₂O volume ratios, (a) 9:1; (b) 8:2; (c) 7:3; (d) 6:4; (e) 5:5; (f) 4:6.

Fig. 5a further showed the XRD pattern of hierarchical porous TiO₂ spheres. Seven well-resolved diffraction peaks, which were well indexed to the 101, 004, 200, 105/211, 204, 116/220, and 215 reflections of anatase, were observed in samples calcinated at 400 °C. The N₂ adsorption-desorption isotherm, as shown in Fig. 5b, showed a type IV curve, which is typical of mesoporous materials, according to the IUPAC nomenclature. The isotherm displayed two hysteresis loops. The hysteresis loop that appeared at low relative pressure between 0.40 and 0.80 was of type H₂. This can be ascribed to capillary condensation in mesopores. The other loop, which appeared at higher pressure, between 0.9 and 1.0, showed a type H₃ shape. These may be caused by the rough texture of the macropore wall surface within the spheres. The BET surface area of these hierarchical porous TiO₂ spheres is $210.6 \text{ m}^2 \text{ g}^{-1}$, which is significantly larger than those of the most reported TiO₂ porous materials (typically around $100 \text{ m}^2 \text{ g}^{-1}$).³³ The BJH pore size distribution curves suggested that this structure has relatively uniform pores with mean size of 5.2 nm. Thus, the as-fabricated hierarchical porous TiO₂ spheres have a

peculiar three levels of pore structure from mesopore to macropore. The hollow TiO₂ spheres and raspberry-like TiO₂ spheres showed similar XRD curves with only anatase phase TiO₂ obtained. Besides, they both exhibited similar N₂ adsorption-desorption isotherm and pore size distribution curves typical for mesoporous materials. The BET surface area and average pore size were 233.8 m² g⁻¹ and 5.0 nm respectively for hollow spheres, and 215.7 m² g⁻¹ and 6.0 nm respectively for raspberry-like spheres. The pore size value for raspberry-like spheres was a little larger than those of hierarchical porous and hollow TiO₂ spheres, possibly because the raspberry-like TiO₂ spheres were assembled from larger TiO₂ primary nanoparticles.

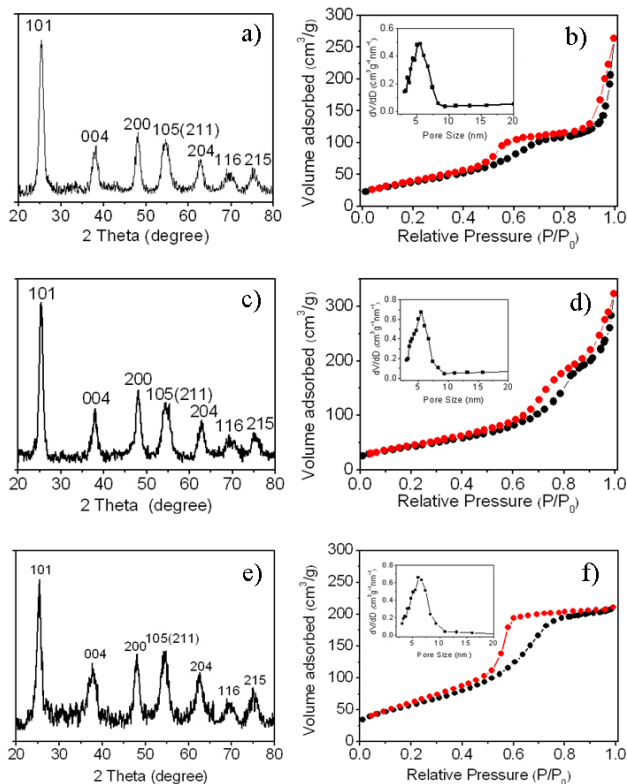
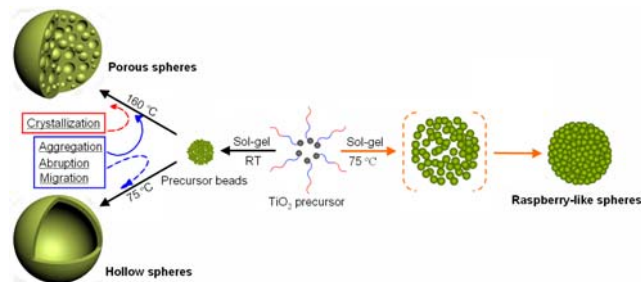


Fig. 5 XRD and nitrogen adsorption/desorption isotherms of a–b) hierarchical porous TiO₂ spheres, c–d) hollow TiO₂ spheres and e–f) raspberry-like TiO₂ spheres.

Formation mechanism of TiO₂ spheres with tunable morphologies.

The formation of hierarchical porous and hollow TiO₂ spheres involves a template-free strategy, but this differs from previously reported template-free mechanisms such as the Ostwald-ripening-method.³⁴ Based on these experimental results and discussions and on the subsequent control experiments, one possible mechanism is deduced, as shown in **Scheme 2**.



Scheme 2. Fabrication of TiO₂ spheres with tunable morphologies.

Like monomeric TiO₂ precursors, when these amphiphilic polymeric hybrid TiO₂ precursors are added to the medium containing water, these precursors will undergo sol-gel process to form TiO₂ inorganic framework. However, due to the special block copolymer segment, these amphiphilic polymer-modified TiO₂ hybrid precursors still have some differences from these monomeric TiO₂ precursors:

i) The long amphiphilic polymer chains tend to self-assemble into organic-inorganic hybrid micelles to reduce the interfacial free energy in the polar solvent.³⁵ This can help to decrease the speed of the Ti groups contacting with water (hydrolysis process) and with other Ti groups (condensation process) and greatly decrease the rate of sol-gel reaction of precursors, rendering the hydrolysis and condensation reactions of TiO₂ precursors to be more controllable. This viewpoint could be proved indirectly from several aspects. First, the typical sol-gel reaction of the monomeric TiO₂ precursors can be run with only about 0.5% water.¹⁵ However, for the amphiphilic polymeric TiO₂ hybrid precursors used in this study, water levels ranging from 10% to 60% by volume needed to be used, as shown in Fig. 2. Second, we also did a contrast experiment by adding the Ti(OiPr)₄ to the PEGHE solution (simple physical mixing) in the mixture of water and ethanol (volume ratio, water: ethanol=1: 9), a macroscopic gelation was observed immediately which is completely different from that of the hydrolysis-condensation behavior of the amphiphilic polymer chemically-modified TiO₂ hybrid precursor used in this study. Third, a typical water soluble polymer, poly(ethylene glycol)-modified TiO₂ precursor, was also synthesized. However, a macroscopic gelation was also observed when water content exceeded 1% by volume. This means that the self-assembly of amphiphilic polymeric TiO₂ hybrid precursors synthesized in this study is essential to the controllable hydrolysis of TiO₂ precursors. The mean sizes of TiO₂ precursor beads were found to be controlled by taking the advantage of different self-assembly behaviors of amphiphilic copolymer segments in different ratios of solvents in the medium.

ii) Because of the reversible hydrolysis reaction and the increase in activation energy caused by the increase in the number of hydrolyzed OR groups, the hydrolysis of TiO₂ precursors does not reach completion even if a large amount of excess water is used. This results in the creation of TiO_a(OH)_b(OR)_{4-2a-b} oxo-polymer structures.³⁶ Since the reaction activity of amphiphilic polymer-modified TiO₂ hybrid precursors used in this study is considerably lower than that of monomeric TiO₂ precursors, it can be deduced that more amphiphilic polymer segments will be inevitably embedded into the TiO₂ precursor beads. This inference can be proved by EDX measurement of the TiO₂ precursor beads, which showed them to contain around 12% carbon and TGA measurement which indicated weight loss as high as 21.3%. The lipophilic interactions between the long-chain alkyl groups of the inorganic-organic composites act as the driving forces to initialize the self-assembly process of the hydrolyzed Ti(OⁱPr)_{3-x}(PEGHE)_{1-y}(OH)_{x+y} species and oligomers to produce TiO₂ precursor beads in the sol-gel synthesis.³⁷

Because the interactions between polymer segments are weaker than the covalent bonds, these polymer-assistant-formed TiO₂ precursor beads had much looser structures than the previously reported TiO₂ spheres made from the monomeric TiO₂ precursors. In this way, these beads may undergo further reaction and rearrangement with the change of external conditions. Specifically, four types of behaviors, including aggregation, abruption, migration, and crystallization of

certain TiO₂ units occurred which led to the formation of TiO₂ with different structures, as discussed in detail as follows.

First, when the as-formed TiO₂ precursor beads further aged at elevated temperatures, further condensation reaction decreased the polymer content on the surfaces of the TiO₂ precursor beads and thus increased the surface energy. This caused the TiO₂ precursor beads to form larger aggregates as we can see the diameters of final TiO₂ spheres were much larger than that of these TiO₂ precursor beads. The decrease of copolymer content on the surface could be proved by XPS. As summarized in **Table 1**, after treatment at 160 °C or 75 °C, the C atomic content dramatically decreased while the Ti atomic content considerably increased, confirming the decrease in surface polymer content after higher temperature treatment. This decrease in surface polymer was also proved by high-resolution of O 1s peak: the increase of O-Ti concentrations and decrease of O-C concentrations of total O atom were clearly observed, as shown in **Fig. S3**.

Table 1. The atom percentages of the as-prepared TiO₂ spheres at different conditions. Sample 1-TiO₂ precursor beads obtained from hydrolysis of TiO₂ precursor at room temperature; Sample 2-sample 1 continued to age at 75 °C for 15 h; Sample 3- sample 1 continued to age at 160 °C for 15 h; Sample 4-TiO₂ precursor beads obtained from hydrolysis of TiO₂ precursor at 75 °C.

Samp.	C % ^a	O%	Ti%	O% (Ti-O) ^b	O% (C-O)
1	70.3	27.0	2.7	18.8	81.2
2	58.4	34.3	7.3	39.8	60.2
3	55.4	36.0	8.6	50.3	49.7
4	53.5	37.5	9.0	48.5	51.5

^a The C, O and Ti atomic percentages based on all elements. ^b Based on all oxygen elements.

Second, high-temperature aging process also caused more polymer segments to be released from the interiors of TiO₂ precursor beads due to the further condensation reaction. EDX measurement revealed 5% and 8% of carbon for 160°C and 75°C treated samples, respectively, which are markedly smaller than that of TiO₂ precursor beads (12%). TGA analyses showed weight loss of 7.9% and 13.7%, respectively for these two samples. These values are also smaller than that of TiO₂ precursor beads (21.3%), indicating a decrease of polymer content in TiO₂ spheres due to the release of polymer segments during aging treatment. Because of the loose and unstable structure of these precursor beads, this release of polymer segments can split the TiO₂ precursor beads into primary TiO₂ nanoparticles during the aging process. To prove this abruption behavior of TiO₂ beads, the as-obtained hierarchical porous and hollow TiO₂ spheres without calcination were treated ultrasonically for 5 h. As shown in **Fig. 6**, only primary TiO₂ nanoparticles around 12 nm in mean diameter remained, indicating that both hierarchical porous and hollow TiO₂ spheres were indeed composed of TiO₂ primary nanoparticles.

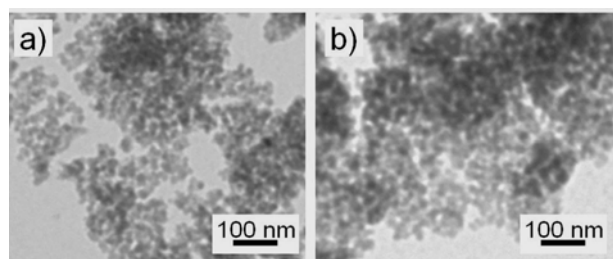


Fig. 6 TEM images of TiO₂ after hierarchical (a) porous and (b) hollow TiO₂ spheres were ultrasonically treated for 5 h.

Third, driven by the minimization of surface energy, smaller, less crystallized, and less dense crystallites from the interiors of TiO₂ precursor beads migrate towards the shell and grow larger, better crystallized, and denser ones.³⁸ The abruption of TiO₂ precursor beads into TiO₂ primary nanoparticles makes the migration process proceed smoothly. Unlike the traditional Ostwald ripening process, in which particles migrated in the form of a dissolved liquid phase, here the units of migration were the TiO₂ primary nanoparticles that make up the final TiO₂ spheres. Besides, the TiO₂ precursor beads can also undergo crystallization during high temperature treatment, which helps to fix the structure of the framework. As a result, the final morphologies of the TiO₂ spheres were determined by the relative rate of above mentioned aggregation, abruption, migration, and crystallization of the TiO₂ precursor beads during aging process.

To further study the relative rate of aggregation, abruption, migration, and crystallization, changes in morphology over time were observed to provide further insight into the reaction kinetics of the high temperature condensation process. As shown in **Fig. 7**, after the TiO₂ precursor beads were held at 160 °C for 10 min, they had already aggregated into larger particles with rough surfaces and irregular shapes, without any primary TiO₂ nanoparticles observed, indicating the rate of aggregation of TiO₂ precursor beads was faster than the rate of abruption. After 2 h, large spherical particles with smooth surfaces formed, indicating the abruption of TiO₂ precursor beads and the rearrangement of TiO₂ primary particles happened. Similar phenomena have also been observed when the aging was conducted at 75 °C. Therefore the difference between the two cases lies in their relative rate of abruption, migration and crystallization under different temperatures. As shown by XRD spectrum in **Fig. 8**, when the aging process was conducted at 160 °C, TiO₂ had a relatively high crystallization rate at this temperature, which helped to fix the framework of the large aggregates to a certain degree. Further hydrolysis-condensation and the release of polymers segments led to the abruption of TiO₂ precursor beads into primary TiO₂ nanoparticles for further migration. As a result, TiO₂ spheres with hierarchical porous structure were formed in the competition of abruption, migration, and crystallization. On the other hand, when the aging was taken place at 75 °C, there was hardly any crystallization of TiO₂. In this case, the abruption of TiO₂ precursor beads and the migration of primary TiO₂ nanoparticles dominated the final morphology. As a result, hollow TiO₂ spheres with mesoporous shell constituted by primary TiO₂ nanoparticles formed.

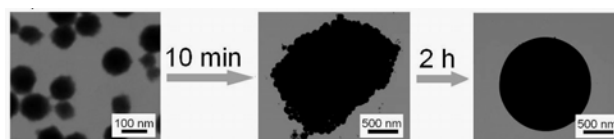


Fig. 7 TEM images of the TiO₂ precursor beads subjected to aging at 160 °C for 10 min and 2 h.

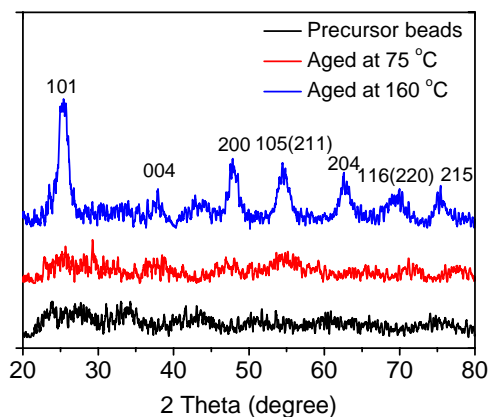


Fig. 8 XRD spectra of the TiO₂ precursor beads, TiO₂ precursor beads after aged at 75 °C for 15 h and TiO₂ precursor beads after aged at 160 °C for 15 h.

The mechanism could be further proved by the formation of raspberry-like TiO₂ spheres. According to the analyses described as above, the formation of these large TiO₂ spherical particles is largely dependent upon the polymer chains on the surfaces and interiors of TiO₂ precursor beads, which have very important impacts on the aggregation and the abruption of the TiO₂ precursor beads. In this way, if the amount of polymer in TiO₂ precursor beads is decreased, the driving force for the abruption and aggregation of TiO₂ precursor beads becomes considerably depressed. Based on this idea, when the temperature of the initial sol-gel reaction of the amphiphilic polymeric TiO₂ hybrid precursors was increased to 75 °C, the raspberry-like TiO₂ spheres were formed.

At elevated temperature, the hydrolysis-condensation reaction becomes violent and the solubility of the copolymers increases. As a result, more polymer chains will dissociate into the medium, leaving fewer polymer segments embedded in the TiO₂ precursor beads. EDX measurements of the TiO₂ precursor beads show around 7% carbon and the TGA measurements showed a weight loss of 12.8%. Both these values are smaller than those of the TiO₂ precursor beads obtained at room temperature (12% and 21.3%, respectively). Besides, XPS scans showed a clear decrease of C atomic content and increase of Ti atomic content, and a decreased of O-C concentrations of total O atom, as shown in Table 1, indicating that the surface polymer content was also lower than that of the TiO₂ precursor beads produced at room temperature. With fewer copolymers regulating the sol-gel process, the hydrolysis-condensation behavior of the amphiphilic polymeric TiO₂ hybrid precursors at 75 °C approached that of the monomeric TiO₂ precursors. The decrease in the polymer on surface and the embedded polymer segments markedly weakens the accumulation and abruption of the TiO₂ precursor beads. In this way, the structures of the TiO₂ precursor beads can be preserved during further aging process at 75 °C (Fig. S4). After calcination, raspberry-like TiO₂ spheres composed of TiO₂ primary nanoparticles were obtained.

Heavy metal ion adsorption properties.

Prompted by their integrated specific hierarchical structures, the as-obtained mesoporous TiO₂ spheres are expected to show promise in the uptake of heavy metal ions for water purification applications. Since Cr (VI) is one of the most toxic pollutants found in the underground water source, in this experiment, Cr (VI) was chosen as the probe to illustrate the adsorption capability of the as-prepared hierarchically nanostructured TiO₂ spheres, and typical commercially available TiO₂ powder (Degussa P-25) was

used for the sake of comparison. The adsorption of Cr (VI) highly depends on the solution pH, and an acidic environment favors their removal.²⁵ Similar phenomenon was observed in this study (Fig. S5). Therefore, the pH values of Cr (VI) initial solutions were adjusted to 3.0 for all the Cr (VI) adsorption experiments.

Fig. 9a shows the typical adsorption isotherms of the as-prepared three kinds of TiO₂ spheres and P25 as a function of Cr (VI) ion concentration. According to the previous reports,³⁹ the Cr (VI) adsorption equilibrium could well fit with Langmuir isotherm model:

$$C_{\text{ads}} = \frac{Q_{\text{max}} b C_{\text{eq}}}{1 + b C_{\text{eq}}}$$

Where C_{ads} (mg/g) and C_{eq} (mg/L) are the equilibrium concentrations of Cr (VI) in the adsorbent and liquid phases, respectively, and b is a Langmuir constant related to the energy and affinity of the sorbent. Q_{max} (mg/g) is the maximum adsorption capacity associated with complete monolayer coverage and used for characterizing the Cr (VI) adsorption capability of the samples. The typical time profiles of Cr (VI) uptake by hierarchical porous TiO₂ with different Cr (VI) ion concentrations were shown in Fig. S6. To eliminate the effect of different equilibrium time needed for Cr (VI) with different concentration, the adsorption experiments were conducted for 24 h to make sure complete adsorption equilibrium to get the value of Q_{max} more accurately. The as-prepared three types of TiO₂ samples all had as high as 13.08, 13.44 and 12.42 mg/g in Q_{max} for hierarchical porous, hollow, and raspberry-like TiO₂ spheres, respectively, which were considerably higher than those of P25 (3.69 mg/g) and the previously reported TiO₂ nanomaterials (less than 10 mg/g), as summarized in Table 2.^{22,25,40} At low pH, the removal of Cr (VI) by TiO₂ should be through the electrostatic interaction between positively charged protonated hydroxyl groups on TiO₂ and various anionic Cr (VI) species (HCrO_4^- , CrO_4^{2-} or $\text{Cr}_2\text{O}_7^{2-}$),^{21,22,25} which was largely determined by surface and pore properties of the materials. The high surface area, narrow pore size distribution and facile mass transportation benefited from the hierarchical nanostructure render the as-prepared TiO₂ spheres to remove Cr (VI) from water more efficiently. Furthermore, the as-prepared TiO₂ samples also readily adsorbed cationic heavy metal ions in solution using Cd (II) adsorption experiment as the example, and the corresponding Q_{max} were 9.28, 9.14 and 8.82 mg/g for hierarchical porous, hollow, and raspberry-like TiO₂ spheres, respectively.

Table 2. Comparison of Q_{max} for Cr (VI) ion removal by different inorganic oxides nanomaterials obtained in the present work and previous reports.

Nanomaterials	Q_{max} (mg/g)	Ref.
Mesoporous TiO ₂ spheres	9.93	22
Micrometer TiO ₂ beads	9.39	25
Sulfated TiO ₂	4.25	40
Mesoporous ZrO ₂ spheres	17.17	22
Mesoporous zirconium titanium oxide spheres	25.40–29.46	22
3D Flowerlike CeO ₂	5.8	26
3D flowerlike iron oxide	3.86–4.47	28
Hierarchical CeO ₂ spheres	6.76	41
Fe ₂ O ₃ @AlO(OH)	21.6	42
Hierarchical TiO ₂ spheres	12.42–13.44	Present work
Commercial TiO ₂ (P-25)	3.69	Present work

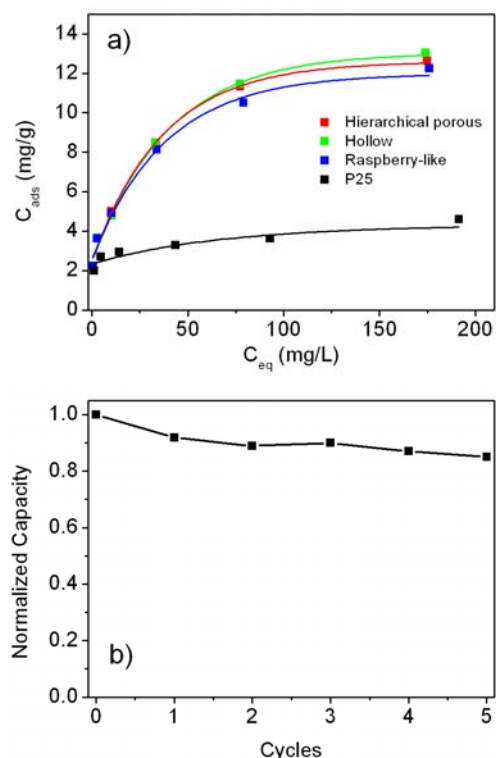


Fig. 9 a) Typical adsorption isotherms of the as prepared mesoporous TiO_2 spheres and P25 with varying compositions. The solid lines are the fitted results using the Langmuir model. b) Regeneration studies of hierarchical porous mesoporous TiO_2 spheres with 5 cycles.

For practical application, the recycling and regeneration of the adsorbent is indispensable, which is also the advantage of transition metal oxides adsorbent compared with traditional adsorbents such as active carbon. Except for their excellent heavy metal ion sequestration performances, the as-prepared TiO_2 could be easily regenerated by treating the Cr (VI)-adsorbed TiO_2 with NaOH solution. As shown in Fig. 9b, with the hierarchical porous TiO_2 spheres as example, the removal efficiency was 92% at the first cycle and then only decreased to 82% after five cycles. Similar results were obtained for TiO_2 with other morphologies, indicating a very good regenerability of these hierarchically nanostructured TiO_2 spheres.

Conclusion

We have demonstrated a facile method for the synthesis of TiO_2 mesoporous spheres with tunable morphologies based on the sol-gel reaction of a novel amphiphilic polymer-modified TiO_2 hybrid precursor. By simply adjusting the conditions of hydrolysis-condensation process, several morphologies, including hierarchical porous, hollow, and raspberry-like TiO_2 spheres can be produced easily. The amphiphilic polymers and their concentrations on the surfaces and interiors of the TiO_2 precursor beads play a vital role in the formation of the tunable morphologies. The as-prepared hierarchically nanostructured TiO_2 spheres have very high adsorption capability for Cr (VI) anion and Cd (II) cation in aqueous solution, showing a high potential for heavy metal ion sequestration and other environmental applications. This study is the first proto and provides an intriguing method to synthesize TiO_2 with tunable

morphologies using amphiphilic polymer to modify monomeric TiO_2 precursors. Due to the wide variety of amphiphilic copolymers with various functional groups and segment lengths and the large number of monomeric inorganic precursors, the present method can readily be extended to the fabrication of TiO_2 and other nanomaterials with specific structures and morphologies. We believe that the method reported here opens new perspectives for facile preparation of inorganic materials with interesting and specific morphologies, since almost all the precursors of inorganic nanomaterials are monomeric and have difficultly controllable sol-gel reactions for tunable morphologies.⁴³

Acknowledgements

Financial support was received from the National Natural Science Foundation of China (Grants 51133001 and 21374018), National "863" Foundation, Science and Technology Foundation of Ministry of Education of China (20110071130002), and Science and Technology Foundation of Shanghai (12nm0503600, 13JC1407800).

Electronic supplementary information (ESI) available: ¹H NMR characterization of the reaction products of $\text{Ti}(\text{OiPr})_4$ with different mole ratio of PEGHE; DLS of the amphiphilic TiO_2 precursors dispersed in different solvent; XPS spectra of the O 1s peak of TiO_2 samples at different preparation stages; TEM and the inserted SEM images of TiO_2 spheres prepared from hydrolysis of amphiphilic TiO_2 precursor at 75 °C at different preparing stage; Effect of initial pH and time profiles of Cr (VI) removal by hierarchical porous TiO_2 . See DOI:

Notes and references

- (a) B. O'Regan and M. Grätzel, *Nature*, 1991, **353**, 737; (b) S. Guldin, S. Hüttner, M. Kolle, M. E. Welland, P. Müller-Buschbaum, R. H. Friend, U. Steiner and N. Tétreault, *Nano Lett.*, 2010, **10**, 2303; (c) S. Wang, K. Wu, E. Ghadiri, M. Lobello, S. Ho, Y. Chi, J. Moser, F. De Angelis, M. Gratzel and M. Nazeeruddin, *Chem. Sci.*, 2013, **4**, 2423.
- (a) H. Tong, S. Ouyang, Y. Bi, N. Umezawa, M. Oshikiri and J. Ye, *Adv. Mater.*, 2012, **24**, 229; (b) W. Sun, S. Zhou, B. You and L. Wu, *Chem. Mater.*, 2012, **24**, 3800.
- (a) X. Feng, J. Zhai and L. Jiang, *Angew. Chem., Int. Ed.*, 2005, **44**, 5115; (b) X. Ding, S. Zhou, G. Gu and L. Wu, *J. Mater. Chem.*, 2011, **21**, 6161; (c) W. Sun, S. Zhou, B. You and L. Wu, *J. Mater. Chem. A*, 2013, **1**, 3146.
- (a) Z. Lu, M. Ye, N. Li, W. Zhong and Y. Yin, *Angew. Chem.*, 2010, **122**, 1906; (b) W. Ma, Y. Zhang, L. Li, L. You, P. Zhang, Y. Zhang, J. Li, M. Yu, J. Guo, H. Lu and C. Wang, *ACS Nano*, 2012, **6**, 3179.
- (a) Q. Wang, X. Guo, L. Cai, Y. Cao, L. Gan, S. Liu, Z. Wang, H. Zhang and L. Li, *Chem. Sci.*, 2011, **2**, 1860; (b) K. Fischer and S. G. Mayr, *Adv. Mater.*, 2011, **23**, 3838.
- J. Lee, M. C. Orilall, S. C. Warren, M. Kamperman, F. J. Disalvo and U. Wiesner, *Nat. Mater.*, 2008, **7**, 222.
- H. Kaper, S. Sallard, I. Djerdj, M. Antonietti and B. Smarsly, *Chem. Mater.*, 2010, **22**, 3502.
- D. Chen, L. Cao, F. Huang, P. Imperia, Y. Cheng and R. A. Caruso, *J. Am. Chem. Soc.*, 2010, **132**, 4438.
- Z. Sun, J. H. Kim, Y. Zhao, F. Bijarbooneh, V. Malgras, Y. Lee, Y.-M. Kang and S. Dou, *J. Am. Chem. Soc.*, 2011, **133**, 19314.
- S. Liu, H. Jia, L. Han, J. Wang, P. Gao, D. Xu, J. Yang and S. Che, *Adv. Mater.*, 2012, **24**, 3201.
- D. Chen and R. A. Caruso, *Adv. Funct. Mater.*, 2013, **23**, 1356.
- X. Chen and S. S. Mao, *Chem. Rev.*, 2007, **107**, 2891.
- Z. Lu and Y. Yin, *Chem. Soc. Rev.*, 2012, **41**, 6874.
- S. Hartmann, D. Brandhuber and N. Husing, *Acc. Chem. Res.*, 2007,

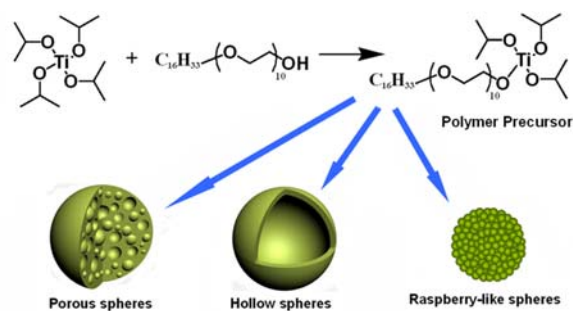
- 40, 885.
- 15 C. Han, R. Luque and D. D. Dionysiou, *Chem. Commun.*, 2012, **48**, 60
1860.
- 16 Y. Mai and A. Eisenberg, *Chem. Soc. Rev.*, 2012, **41**, 5969.
- 5 17 Y. Mai and A. Eisenberg, *Acc. Chem. Res.*, 2012, **45**, 1657.
- 18 S. Eiden-Assmann, J. Widoniak and G. Maret, *Chem. Mater.*, 2004,
16, 6. 65
- 19 (a) B. Z. Tian, X. Liu, B. Tu, C. Yu, J. Fam, L. Wang, S. H. Xie, G. D.
Stucky and D. Zhao, *Nat. Mater.*, 2003, **2**, 159; (b) J. Zhang, Y. Deng,
10 D. Gu, S. Wang, L. She, R. Che, Z. Wang, B. Tu, S. Xie and D. Zhao,
Adv. Energy Mater., 2011, **1**, 241.
- 20 H. Wang, G. Agrawal, L. Tsarkova, X. Zhu and M. Möller, *Adv. Mater.*, 70
2013, **25**, 1017.
- 21 J. Hu, L. Zhong, W. Song and L. Wan, *Adv. Mater.*, 2008, **20**, 2977.
- 15 22 D. Chen, L. Cao, T. L. Hanley and R. A. Caruso, *Adv. Funct. Mater.*,
2012, **22**, 1966.
- 23 J. Choi, A. Ide, Y. B. Truong, I. L. Kyratzis and R. A. Caruso, *J. Mater.* 75
Chem. A 2013, **1**, 5847.
- 24 L. Zhong, J. Hu, L. Wan and W. Song, *Chem. Commun.*, 2008, 1184.
- 20 25 N. Wu, H. Wei and L. Zhang, *Environ. Sci. Technol.*, 2012, **46**, 419.
- 26 L. Zhong, J. Hu, A. Cao, Q. Liu, W. Song and L. Wan, *Chem. Mater.*,
2007, **19**, 1648. 80
- 27 Z. Ai, Y. Cheng, L. Zhang and J. Qiu, *Environ. Sci. Technol.*, 2008, **42**,
6955.
- 25 28 L. Zhong, J. Hu, H. Liang, A. Cao, W. Song and L. Wan, *Adv. Mater.*,
2006, **18**, 2426.
- 29 T. K. Kim, K. J. Lee, J. Y. Cheon, J. H. Lee, S. H. Joo and H. R. Moon, 85
J. Am. Chem. Soc., 2013, **135**, 8940.
- 30 N. D. Petkovich and A. Stein, *Chem. Soc. Rev.*, 2013, **42**, 3721.
- 30 31 W. Li, Z. Wu, J. Wang, A. A. Elzatahry and D. Zhao, *Chem. Mater.*,
2014, **26**, 287.
- 32 X. Zhang, T. Ma and Z. Yuan, *J. Mater. Chem.*, 2008, **18**, 2003. 90
- 33 (a) D. Chen, F. Huang, Y. Cheng and R. A. Caruso, *Adv. Mater.*, 2009,
21, 2206; (b) Y. J. Kim, M. H. Lee, H. J. Kim, G. Lim, Y. S. Choi, N.-
35 G. Park, K. Kim and W. I. Lee, *Adv. Mater.*, 2009, **21**, 3668.
- 34 (a) H. Li, Z. F. Bian, J. Zhu, D. Zhang, G. Li, Y. Huo, H. Li and Y. Lu,
J. Am. Chem. Soc., 2007, **129**, 8406; (b) J. Hu, M. Chen, X. Fang and
95 L. Wu, *Chem. Soc. Rev.*, 2011, **40**, 5472.
- 35 P. T. Tanev, M. Chibwe and T. J. Pinnavaia, *Nature*, 1994, **368**, 321.
- 40 36 (a) J. Blanchard, S. Barboux-Doeuff, J. Maquet and C. Sanchez, *New*
J. Chem., 1995, **19**, 929; (b) J. Blanchard, B. Schaudel and C. Sanchez,
100 *Eur. J. Inorg. Chem.*, 1988, 1115.
- 37 (a) A. Monnier, F. Schüth, Q. Huo, D. Kumar, D. Margolese, R. S.
Maxwell, G. D. Stucky, M. Krishnamurty, P. Petroff, A. Firouzi, M.
45 Janicke and B. F. Chmelka, *Science*, 1993, **261**, 1299; (b) I. M.
Arabatzi and P. Falaras, *Nano Lett.*, 2003, **3**, 249.
- 38 J. Li and H. C. Zeng, *J. Am. Chem. Soc.*, 2007, **129**, 15839. 105
- 39 G. L. Drisko, V. Luca, E. Sizgek, N. Scales and R. A. Caruso,
Langmuir, 2009, **25**, 5286.
- 50 40 F. Jiang, Z. Zheng, Z. Y. Xu, S. R. Zheng, Z. B. Guo and L. Q. Chen, *J.*
Hazard. Mater., 2006, **134**, 94.
- 41 H. Xiao, Z. Ai and L. Zhang, *J. Phys. Chem. C*, 2009, **113**, 16625. 110
- 42 X. Yang, X. Wang, Y. Feng, G. Zhang, T. Wang, W. Song, C. Shu, L.
Jiang and C. Wang, *J. Mater. Chem. A*, 2013, **1**, 473.
- 55 43 N. Pinna and M. Niederberger, *Angew. Chem. Int. Ed.*, 2008, **47**, 5292.

125

130

TOC

5



Hierarchically nanostructured TiO₂ spheres with tunable morphologies and excellent heavy metal ion
10 sequestration performances were fabricated from an amphiphilic polymer/inorganic precursor.

15